Modelling of Charging Control Scheme
for QZSI with Battery Topology

KAH-HAW LAW
Department of Electronic and Computer Engineering
Curtin University Malaysia
CDT 250, 98009 Miri, Sarawak, Malaysia
E-mail: lawkahhaw@curtin.edu.my

Quasi Z-source inverter (qZSI) has been proven to be reliable for inverting DC electricity to AC. When compared with conventional two stage DC-AC boost inverter topology, qZSI is a single stage topology which can be simply constructed via connecting a quasi Z-source (qZS) impedance network in series with an H-bridge inverter. This resulted an attractive topology without needing any switching element and resistor in the DC-link. In this paper, the investigation of qZSI with battery topology is extended to regulate its output voltage from a fluctuating DC input source. Through extensive mathematic derivation, a control scheme which comprised of battery current controller, battery management algorithm, and electronic circuit breaker (ECB) algorithm, is proposed to achieve the aforementioned outcome plus ensuring the effectiveness of battery charging and discharging capability as well as prevention of over-charging and over-discharging of the battery according to the DC input voltage level. All theoretical findings are validated with simulation results using Matlab / Simulink software package.

Keywords: quasi Z-source inverter (qZSI), battery current controller, battery management, electronic circuit breaker (ECB), carrier based pulse width modulation technique (CBPWM)

1. INTRODUCTION

Nowadays, renewable energy sources have been widely exploited due to inadequacy of the global fossil fuel and increase of environmental impacts such as air pollution, global warming, *etc.* [1]. There are several renewable energy resources available such as solar, wind, hydro and biomass. Currently, there are about 19% of the electricity energy generation is using renewable energy and it is estimated to reach 30% by 2030 [2]. Moreover, the integration of (photovoltaic) PV in various systems is becoming more popular when compared to other renewable sources. This can be realized from the rapid growth in global installed capacity for solar-powered electricity due to the technological improvements in solar energy and the decrement in cost. However, the output voltage produced from the PV panel is unstable due to the variations of irradiance and temperature [3]. To counter this issue, battery energy storage system (BESS) is introduced to the PV system to provide smooth and stable power to grid/load [4]. BESS can also store the redundant energy or supply the excessive energy to the load. On the other hand, power converters and inverters play important role for the PV-battery system. The traditional two stage topologies, which structured by cooperating any DC-DC converter with an inverter, are commonly used to regulate and boost the PV voltage up to a desired level before proceeding the inverting action. However, due to the extra switch presented in the DC stage, complex controller and high construction cost are normally borne by these conventional topologies [5-7].

The existence qZSI overcomes the aforementioned issues and has several advantages over the conventional ZSI such as low voltage stress [8-11]. The qZSI can perform buck-boost operation in a single stage topology with lower I^2R loss and higher efficiency. It can also be controlled to achieve four quadrant operation. For instance, [12] proposed a new PV grid-tie qZSI topology with battery energy storage system that ensures desired stable grid power generation. The battery was paralleled with the non DC-link capacitor in the qZS network. An energy management control scheme, which consists of PI controllers and maximum power point tracking (MPPT) algorithm, was also established to control the topology while taking the power regulation, storage, and safety of the battery into consideration. However, the switching frequency of the sinusoidal pulse width modulation (SPWM) technique was not revealed. The aforementioned topology was utilized in [13] to smoothen the grid-injected power. The SOC of the battery was managed via the PI based current double loop controller. To overcome the non-linear characteristic and to ease the controller design, the small-signal dynamic model of the proposed topology was established so that a linear system near the steady-state operating point can be approximated. In addition, the switching elements of the proposed topology were driven by the gate drive signals produced via the modified space vector PWM technique. Nevertheless, no switching frequency was revealed from the work. The work demonstrated in [13] was extended in [14] with P-Q decoupling controller to achieve unity power factor. The multilevel cascaded qZSI with batteries was first deputed in [15] as a PV grid-tie power system. Besides incorporating all aforementioned control scheme (*i.e.*, battery energy management and MPPT control), the proportional and resonant (PR) controller was employed as grid current control to ensure the grid operating at unity power factor. In addition, the proposed control scheme, together with phase-shift SPWM (PS-SPWM) switching at 10 kHz, could achieve power balancing in different qZSI modules. With conventional battery management framework, [16] proposed a control scheme for the PV grid-tie qZSI topology with battery that works in both grid-connected and islanded modes of microgrid operation. Specifically, the control scheme consisted of one PR based AC current controller and another PR based AC voltage controller, which were designed to improve power factor correction (*i.e.*, in grid-connected mode) and provide harmonics compensation (*i.e.*, in islanded mode), respectively, in power system. On the other hand, although the effective switching frequency was given as 10 kHz, but the modulation technique used to drive the topology was not discussed. The work demonstrated in [15] were further enhanced in [17] for the seven-level cascaded qZSI with batteries. The proposed control scheme not only limited all the batteries from over-charging and over-discharging, but also controlled them to operate in the same SOC. As a result, all batteries can be efficiently utilized and last longer.

This paper focused on developing a control scheme for the qZSI with battery topology [18]. The control scheme, which consists of novel algorithms, ensures charging and discharging the battery as well as preventing it from over-charging and over-discharging. The proposed controller also regulates the DC-link voltage in regardless to the changes of DC input voltage. Furthermore, unipolar carrier based pulse width modulation technique is employed in this work to attain the single-phase AC output voltage waveform. The paper is arranged in the following order: Section 2 elaborates the operation of the proposed qZSI and its small-signal model. Section 3 demonstrates the design implementation of the battery current controller, battery management algorithm, and ECB algorithm in detail. Simulation results are analyzed, discussed, and presented in Section 4. Lastly, conclusions are made in Section 5.

2. MODELLING OF QZSI WITH BATTERY

2.1 Proposed Energy Stored Quasi Z-Source Inverter System

Fig. 1 shows the circuitry of the proposed qZSI topology for small signal analysis where one battery is connected in parallel to the DC capacitor C_2.
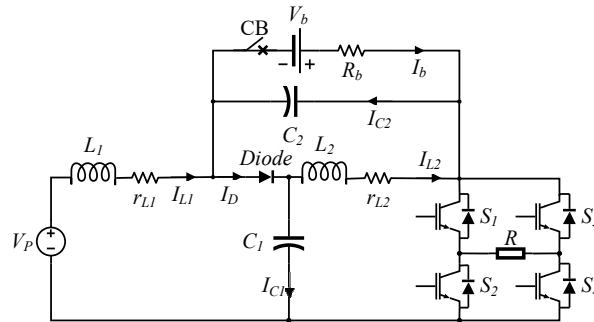
Fig. 1. Small-signal model of the qZSI with battery topology.

Similar to the traditional qZSI, the proposed topology has two operating states; namely the shoot through state and the non-shoot through state. During shoot through state, cross conduction occurs through each phase leg of the IGBT H-bridge inverter causing the diode to be reverse biased as well as the capacitors energize its respective inductors. Whereas during non-shoot state, the conduction across S_1 and S_4 or S_2 and S_3 of the H-bridge inverter forced the diode to be forward biased. This allows both the DC input voltage and inductors to discharge in order to charge up the capacitors and drive the load simultaneously.

The state equations of the proposed qZSI (*i.e.*, for both the shoot through state D and non-shoot through state $1-D$) are detailed in [19] together with the relationship of the parameters found in Fig. 1. Particularly, V_P defines the DC input voltage, V_{C1} and V_{C2} are the voltages measured across capacitor C_1 and C_2, respectively, I_{L1} and I_{L2} are the currents flowing through inductor L_1 and L_2, respectively, and V_{PN} is the DC-link voltage.

2.2 Small-Signal Model of Proposed qZSI

For simplicity, the equivalent series resistance (ESR) of each inductor is considered while the ESR of all the capacitors are ignored. Due to the versatility of the proportional regulator present in the design of the battery current controller, the feasibility of the controller can be ensured despite the absence of capacitor's ESR [1]. The battery V_b with its internal resistance R_b is connected in parallel to the DC capacitor C_2; indicating that the voltage is the same across each path of the parallel circuit. The relationship between the voltage of battery V_b and capacitor V_{C2} are defined in Eqs. (1) and (2) as below:

$$V_{C2} = V_b = V_{OCV} - R_b I_b, \tag{1}$$

$$\dot{V}_{C2} = -R_b \dot{I}_b. \tag{2}$$

where I_b defines the current flows through the battery and V_{OCV} defines the DC voltage measured across the battery.

By assuming identical of inductors' stray resistances, the state space equations for the shoot through state and non-shoot through state are attained in Eqs. (3) and (4), respectively, in matrix form as follows:

$$\begin{bmatrix} L \\ L \\ C \\ -R_b C \end{bmatrix}\begin{bmatrix} \iota'_{L1} \\ \iota'_{L2} \\ v'_{C1} \\ \iota'_b \end{bmatrix} = \begin{bmatrix} -r_L & 0 & 0 & -R_b \\ 0 & -r_L & 1 & 0 \\ 0 & -1 & 0 & 0 \\ -1 & 0 & 0 & 1 \end{bmatrix}\begin{bmatrix} i_{L1} \\ i_{L2} \\ v_{C1} \\ i_b \end{bmatrix} + \begin{bmatrix} 1 & 0 & 1 \\ 0 & 0 & 0 \\ 0 & 0 & 0 \\ 0 & 0 & 0 \end{bmatrix}\begin{bmatrix} v_P \\ i_{PN} \\ v_{OCV} \end{bmatrix},$$

(3)

$$\begin{bmatrix} L \\ L \\ C \\ -R_b C \end{bmatrix}\begin{bmatrix} \iota'_{L1} \\ \iota'_{L2} \\ v'_{C1} \\ \iota'_b \end{bmatrix} = \begin{bmatrix} -r_L & 0 & -1 & 0 \\ 0 & -r_L & 0 & R_b \\ 1 & 0 & 0 & 0 \\ 0 & 0 & 0 & 0 \end{bmatrix}\begin{bmatrix} i_{L1} \\ i_{L2} \\ v_{C1} \\ i_b \end{bmatrix} + \begin{bmatrix} 1 & 0 & 0 \\ 0 & 0 & -1 \\ 0 & -1 & 0 \\ 0 & -1 & 0 \end{bmatrix}\begin{bmatrix} v_P \\ i_{PN} \\ v_{OCV} \end{bmatrix}.$$

(4)

The aforementioned equations are converted to an average dynamic state space equation after substituting d and $1 - d$ into Eqs. (3) and (4), respectively, followed by equating them as given by:

$$\begin{bmatrix} L \\ L \\ C \\ R_b C \end{bmatrix}\begin{bmatrix} \iota'_{L1} \\ \iota'_{L2} \\ v'_{C1} \\ \iota'_b \end{bmatrix} = \begin{bmatrix} -r_L & 0 & d-1 & -dR_b \\ 0 & -r_L & 0 & (1-d)R_b \\ 1-d & -d & 0 & 0 \\ d & d-1 & 0 & -1 \end{bmatrix}\begin{bmatrix} i_{L1} \\ i_{L2} \\ v_{C1} \\ i_b \end{bmatrix} + \begin{bmatrix} 1 & 0 & d \\ 0 & 0 & d-1 \\ 0 & d-1 & 0 \\ 0 & 1-d & 0 \end{bmatrix}\begin{bmatrix} v_P \\ i_{PN} \\ v_{OCV} \end{bmatrix}.$$

(5)

Consider steady-state conditions only, Eq. (5) is simplified by ignoring its left-hand side terms to yield the relationship between the variables as shown below:

$$v_{C1} = \frac{1-d}{1-2d}v_p + \frac{-r_L(1-d)i_{PN} + r_L d i_b}{1-2d},$$

(6)

$$v_{C2} = v_b = \frac{d}{1-2d} + \frac{-r_L(1-d)i_{PN} + r_L d i_b}{1-2d},$$

(7)

$$i_{PN} = \frac{(1-2d)i_{L1} + d i_b}{1-d}.$$

(8)

After taking Laplace transform onto Eq. (5), the dynamic small-signal model of the qZSI with battery topology is acquired and is represented via Eqs. (9)-(11) after taking the small deviations of state variables from an operating point into consideration [19-26].

$$(L_s + r_L)\widetilde{i_{L1}}(s) = (d-1)\widetilde{v_{C1}}(s) + \widetilde{v_P}(s) - dR_b\widetilde{i_{C1}}(s) + (V_{C1} - R_b I_b + V_{ocv})\tilde{d}(s)$$

(9)

$$C_s\widetilde{v_{C1}}(s) = (1-2d)\widetilde{i_{L1}}(s) + d\widetilde{i_b}(s) + (d-1)\widetilde{i_{PN}}(s) + (I_{PN} - 2I_{L1} + I_b)\tilde{d}(s)$$

(10)

$$(R_b C_s + d)\tilde{\imath}_b(s) = (2d-1)\widetilde{\imath_{L1}}(s) + (1-d)\widetilde{\imath_{PN}}(s) + (I_{PN} - 2I_{L1} + I_b)\tilde{d}(s) \tag{11}$$

where each lower-case variable with tilde (*e.g.*, $\tilde{a}_a$) defines the small-signal perturbation, each upper-case variable (*e.g.*, A_a) defines the steady-state operating point, and $d(s)$ is the steady-state shoot through duty ratio.

By Eqs. (9)-(11), the transfer function that relates the battery current $\tilde{\imath}_{(s)}$ with the small perturbation of steady-state shoot through duty ratio $\tilde{d}_{(s)}$ around its steady-state operating point is obtained as follows:

$$G_{\tilde{\imath}_b,\tilde{d}} = \frac{\tilde{\imath}_b(s)}{\tilde{d}(s)} = \frac{(2D-1)(V_{C1} - R_b I_b + V_{ocv}) + (-L_s - r_L)(I_{PN} - 2I_{L1} + I_b)}{CLR_b s^2 + (CR_b r_L + DL)s + Dr_L + R_b(1-2D)^2}. \tag{12}$$

3. CONTROL SCHEME

Fig. 2 depicts the single-phase qZSI with battery topology controlled by the proposed control scheme which is formed by the combination of battery current controller, battery management algorithm, and battery ECB algorithm.

3.1 Battery Current Controller

Fig. 2 also illustrates the block diagram of the battery current controller for the qZSI with battery topology.
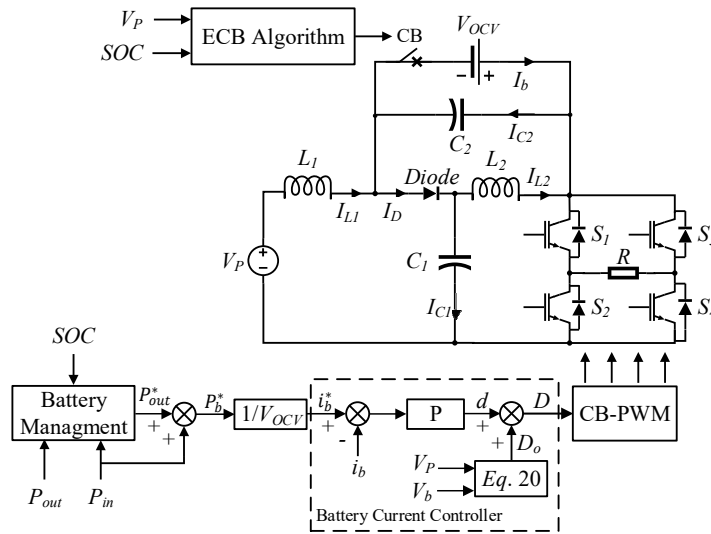
Fig. 2. The qZSI with battery topology controlled by the proposed control scheme.

The role of the battery current controller is to manage the power of the battery by producing the desired shoot-through duty ratio. After the P_{out}^* produced from the battery management algorithm is fed into the battery current controller, it will subtract the input

power P_{in} to produce the reference battery power P_b^*. The reference battery power will then undergo power law equation $P = IV$ and the reference battery current i_b^* is produced. The current loop is controlled via proportional (P) controller in order to obtain the small perturbation of steady-state shoot through duty ratio d. On the other hand, a feed-forward controller is employed to get the steady-state shoot through duty cycle D_o given by:

$$D_o = \frac{V_b}{V_P - 2V_b}.$$
(13)

The summation of the steady-state and the small perturbation of steady-state shoot through duty ratio yields the final shoot through duty cycle D, which is fed to the CB-PWM modulator to achieve simple boost control.

3.2 Battery Management Framework

Fig. 3 demonstrates the battery management framework for the qZSI with battery topology which is implemented to ensure that the battery is able to charge or discharge effectively. The DC input power P_{in} and the DC output power P_{out} are derived in Eqs. (14) and (15), respectively.

$$P_{in} = V_P \times I_{L1}$$
(14)

$$P_{out} = V_{PN} \times I_{PN}$$
(15)
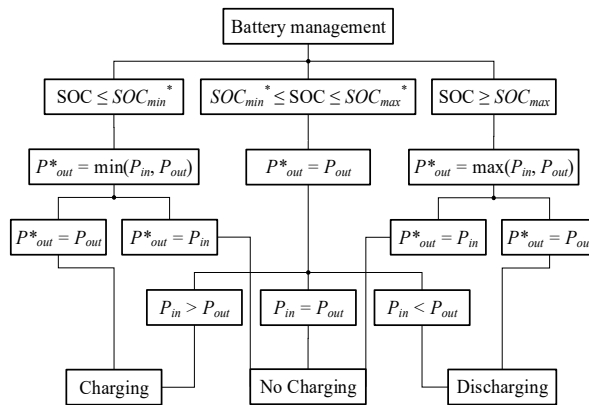
Fig. 3. Battery management algorithm.

The aforementioned power variables are fed into the state of charge (SOC) controller for comparison purpose in order to produce the output reference power P_{out}^* which derived below:

$$P_{out}^* = P_{out} - P_{in}.$$
(16)

Besides, the battery reference power, P_b^* in the controller can be obtained in Eq. (17) given by:

$$P_b^* = P_{out}^* - P_{in}. \tag{17}$$

From Fig. 3, the battery status is separated into three cases, which are (1) $P_{in} > P_{out}$; (2) $P_{in} = P_{out}$; and (3) $P_{in} < P_{out}$. By referring to Eqs. (16) and (17), the battery status based on the aforementioned cases can be justified. In the first case, the current flows through L_2 is larger than the one through L_1 (*i.e.*, $I_{L1} < I_{L2}$). This yields the battery power $P_b < 0$ W (*i.e.*, charging); causing the redundant power to be absorbed by the battery. In the second case, the current flows through each inductor L_1 and L_2 has the same amplitude (*i.e.*, $I_{L1} = I_{L2}$); hence, resulting the battery power $P_b = 0$ W (*i.e.*, no charging). Conversely in the last case, $I_{L1} > I_{L2}$ initiates the stored battery power (*i.e.*, $P_b > 0$ W) to be released (*i.e.*, discharging) and outputted to the load.

The battery status is obtained by referring to its SOC. Fig. 3 illustrates the battery management algorithm, where SOC_{max}^* and SOC_{max}^* are referring to the maximum and minimum of the presumed SOC of the battery, respectively. In another words, the battery cannot be over-charged above SOC_{max}^* or over-discharged below SOC_{min}^*. For instance, if the SOC of battery is lower than SOC_{min}^*, the battery stays idle when $P_{out}^* = P_{in}$ (*i.e.*, $P_b^* = 0$ in Eq. (17)). However, if $P_{out}^* = P_{out}$ (*i.e.*, $P_b^* < 0$), the battery will charge. If the SOC of battery is above SOC_{max}^*, the battery cannot be charged when $P_{out}^* = P_{in}$ (*i.e.*, $P_b^* = 0$). However, if $P_{out}^* = P_{out}$ (*i.e.*, $P_b^* > 0$), the battery will discharge. When the SOC of battery falls within the range between SOC_{min}^* and SOC_{max}^*, the battery can be charged or discharged depending on the qZSI input power P_{in}.

3.3 Battery Electronic Circuit Breaker Algorithm

A series-connected ECB with the battery is proposed to protect the lifespan of the battery by preventing it from over-charging and over-discharging. Fig. 4 illustrates the algorithm of the ECB. From Fig. 4, the ECB algorithm is structured to output two states (*i.e.*, 0 = normally open (NO) and 1 = normally closed (NC)) according to the battery SOC, the DC input voltage V_P, the preferred battery SOC (*i.e.*, SOC_{min}^* and SOC_{max}^*), and the DC input voltage references (*i.e.*, V_P^* and V_P^{**}). For this work, considering that lithium-ion battery used in electric vehicle will be utilized in the qZS network, hence, SOC_{min}^* and SOC_{max}^* is set at 41% and 79%, respectively while V_P^* and V_P^{**} is set at 11V and 13V, respectively [27]. The aforementioned constraints ensure the battery stays idle when its SOC has reached the upper or lower limit.
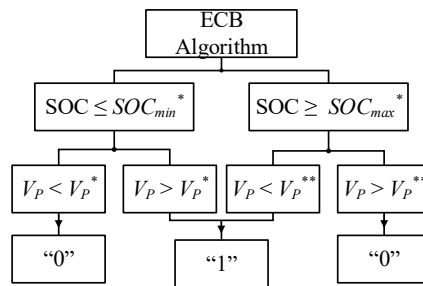
Fig. 4. Electronic circuit breaker algorithm.

For instance, the initial state of the ECB is in NC state (*i.e.*, 1); indicating that the battery is connected in parallel to the DC capacitor C_2. When the algorithm detects the battery SOC and the DC input voltage V_P are greater than the maximum reference values (*i.e.*, SOC^*_{max} and V_P^{**}), ECB will become '0'. Similarly, ECB will change to '0' too when the the battery SOC and the DC input voltage V_P are both smaller than the minimum reference values (*i.e.*, SOC^*_{min} and V_P^*).

4. SIMULATION RESULTS

The proposed battery current controller, battery management framework, and ECB algorithm for the single-phase qZSI with battery topology were tested through intensive simulation using MATLAB/SIMULINK. There were three scenarios to be investigated: (1) the charging and discharging regimes of battery; (2) the over-charge prevention of battery; and (3) the over-discharge prevention of battery. The run time for the simulation was 1.5 s. Table 1 tabulated all the parameters while Table 2 shown the specific battery parameters used in the simulation. Lead-acid battery is used for this work due to its widely availability in practice with cheaper cost and durability as compared to lithium-ion battery. The rated capacity is set as 0.1 Ah to shorten the simulation time. Specifically, the battery current and its rated capacity affect its discharging time as shown in Eq. (18) below.

$$Battery\ discharge\ time = \frac{Rated\ capacity}{Battery\ current} \tag{18}$$

Table 1. System parameters.

Circuit parameters	Value
DC input voltage V_P	6 V, 12 V, 24 V
Battery internal resistor R_b	0.17 Ω
Inductance of L_1 and L_1	100 μH
Internal resistance of inductor r_1 and r_2	0.15 Ω
Capacitance of C_1 and C_2	1000 μF
Load resistor R	52 Ω
Fundamental frequency	50 Hz
Switching frequency	40 kHz

Table 2. Battery parameters.

Parameters	Value
Type	Lead-Acid
Nominal voltage	12 V
Rated capacity	0.1 Ah
Maximum capacity	0.10417 Ah
Cut-off voltage	9 V
Full charged voltage	13.07 V
Nominal discharge current	0.02 A
Internal resistance	1.2 Ω
Capacity at nominal voltage	0.031 Ah

4.1 Charging and Discharging Regimes of Battery

In this scenario, the SOC of the battery was set to 50 % while a step change of DC input voltage V_P from 24 V to 6 V was introduced at 0.75 s to examine the charging and discharging behavior of the battery under the same loading condition.

Specifically, Fig. 5 (a) demonstrated that, from 0 s to 0.75 s, the battery absorbed the redundant energy from the DC input voltage V_P while in contrast, the battery was discharged from 0.75 s to 1.5 s to provide energy support to the load. The aforementioned phenomena can be realized in Fig. 5 (c) where the DC output power P_{out} was lower and higher than the DC input power P_{in} during 0 s to 0.75 s and 0.75 s to 1.5 s, respectively.

Fig. 5 (b) depicted the relationship between the DC currents (*i.e.*, I_b, I_{L1}, and I_{L2}) which can be verified in [19] while Fig. 5 (d) shown the resultant steady-state shoot through duty cycle via Eq. (13) to affirm the aforementioned step change of DC input voltage V_P. The aforementioned results can be summarized in Table 3 below.
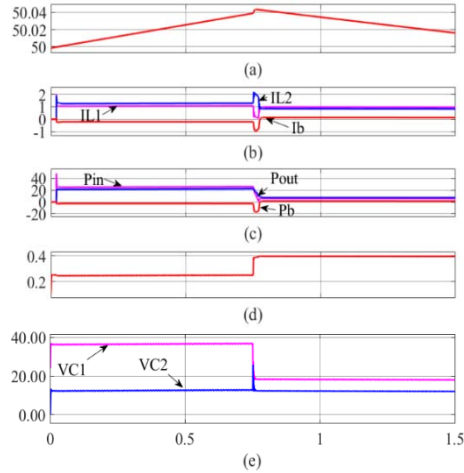
Fig. 5. Simulation results when $SOC^*_{min} \leq$ SOC $\leq SOC^*_{max}$; (a) battery SOC; (b) battery current I_b and inductors' currents I_{L1} and I_{L2}; (c) DC input power P_{in}, DC output power P_{out}, and battery power P_b; (d) shoot-through duty ratio D; and (e) DC capacitors' voltages V_{C1} and V_{C2}.
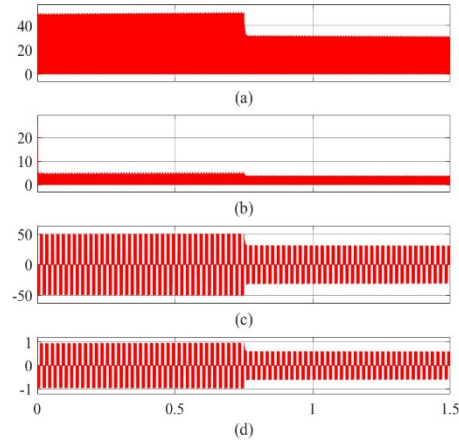
Fig. 6. Simulation results of (a) DC-link voltage V_{PN}; (b) DC-link current $I_{PN;}$ (c) AC voltage v_o; and (d) AC current i_o.

Table 3. Status of battery power and inductor currents.

Power relationship	Battery Power and Status	Inductor Currents
$P_{in} > P_{out}$	$P_b < 0$, Charging	$I_{L2} > I_{L1}$
$P_{in} < P_{out}$	$P_b > 0$, Discharging	$I_{L2} < I_{L1}$

Furthermore, Fig. 6 illustrated that the DC-link voltage is able to achieve steady state without being affected by the transition of DC input voltage.

4.2 Over-Charge Prevention of Battery

In this scenario, the SOC of the battery was set to 80 % while two step changes of DC input voltage V_P from 12 V to 24 V followed by 6 V were executed at 0.5 s and 1 s, respectively, to examine the charging and discharging behavior of the battery under the same loading condition. These step changes can be realized by Eq. (13) as depicted in Fig. 7. Fig. 7 (a) illustrated that, from 0 s to 0.5 s (*i.e.*, $V_P = 12$ V), the ECB was in NO state and and the battery SOC remained the same at 80% with zero amplitude of battery current I_b (see Fig. 7 (b)) and battery power P_b (see Fig. 7 (c)).

The aforementioned phenomenon was also realized from 0.5 s to 1 s (*i.e.*, $V_P = 24$ V) when the battery SOC reached SOC^*_{max}; disconnecting the battery from the circuit via ECB.

After 1 s (*i.e.*, $V_P = 6$ V), the ECB commenced to NC state causing the battery to discharge (*i.e.*, SOC decrease) with positive amplitude of battery current I_b and battery power P_b to offer energy support to the load.

Fig. 8 shows the DC voltages measured across the DC capacitors in the qZS network. It can be observed that V_{C1} is always greater than V_{C2}.

Fig. 8. Simulation results of DC capacitors' voltages V_{C1} and V_{C2}.
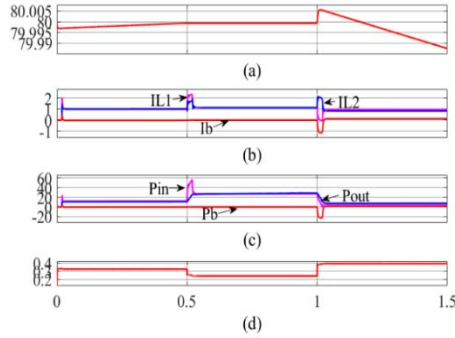
Fig. 7. Simulation results of SOC $\geq SOC^*_{max}$; (a) battery SOC; (b) battery current I_b and inductors' currents I_{L1} and I_{L2}; (c) DC input power P_{in}, DC output power P_{out}, and battery power P_b; and (d) shoot-through duty ratio D.
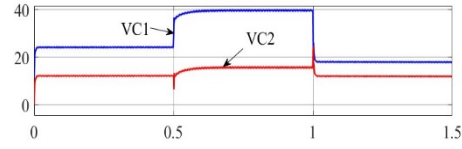
4.3 Over-Discharge Prevention of Battery

In this scenario, the SOC of the battery was set to 40 % with similar of two step changes of DC input voltage V_P. Fig. 9 (a) illustrated that, from 0 s to 0.5 s (*i.e.*, $V_P = 12$ V), the ECB was in NO state and the battery SOC remained the same at 40% with zero amplitude of battery current I_b (see Fig. 9 (b)) and battery power P_b (see Fig. 9 (c)).

At 0.5 s to 1 s (*i.e.*, $V_P = 24$ V), the ECB closed and the battery was charged with linear rate. This charging scenario can be realized from the negative amplitude of battery current I_b (see Fig. 9 (b)) and battery power P_b (see Fig. 9 (c)). After 1 s (*i.e.*, $V_P = 6$ V), the ECB resumed back to NO state causing the battery to remain at 40 % with zero ampli-

Fig. 10. Simulation results of DC capacitors' voltages V_{C1} and V_{C2}.
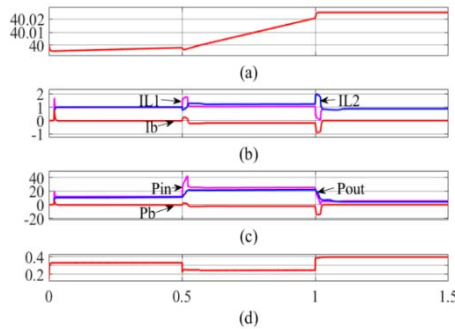
Fig. 9. Simulation results of SOC $\leq SOC^*_{min}$; (a) battery SOC; (b) battery current I_b and inductors' currents I_{L1} and I_{L2}; (c) DC input power P_{in}, DC output power P_{out}, and battery power P_b; and (d) DC capacitors' voltages V_{C1} and V_{C2}.
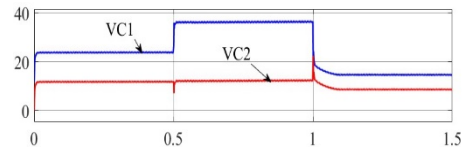
tude of battery current I_b and battery power P_b. Fig. 10 depicts the DC voltages measured across the DC capacitors in the qZS network.

5. CONCLUSIONS

This paper proposed a control scheme for single-phase qZSI with battery topology. The proposed control scheme is structured with battery current controller, battery management algorithm, and the ECB algorithm in Matlab/Simulink. Specifically, the battery current controller is designed to control the battery current in qZSI. On the other hand, the battery management algorithm and ECB algorithm are implemented to prevent the battery from over over-charging or over-discharging in the qZS network. All mathematical equations for the topology and the proposed scheme were derived and verified through simulation results. It is concluded that the battery is able to effectively charge and discharge as well as protecting it from over-charging and over-discharging.

REFERENCES

1. K. H. Law, M. S. A. Dahidah, and N. Mariun, "Cascaded multilevel inverter based statcom with power factor correction feature," in *Proceedings of IEEE Conference on Sustainable Utilization and Development in Engineering and Technology*, 2011, pp. 12-18.
2. K. H. Law, M. S. A. Dahidah, and H. A. F. Almurib, "SHE-PWM cascaded multilevel inverter with adjustable DC voltage levels control for STATCOM applications," *IEEE Transactions on Power Electronics*, Vol. 29, 2014, pp. 6433-6444.
3. K. H. Law, M. S. A. Dahidah, G. S. Konstantinou, and V. G. Agelidis, "SHE-PWM cascaded multilevel converter with adjustable DC sources control for STATCOM applications," in *Proceedings of the 7th International Power Electronics and Motion Control Conference*, 2012, pp. 330-334.
4. K. H. Law and M. S. A. Dahidah, "DC-DC boost converter based MSHE-PWM cascaded multilevel inverter control for STATCOM systems," in *Proceedings of International Power Electronics Conference*, 2014, pp. 1283-1290.
5. K. H. Law and M. S. A. Dahidah, "New current control algorithm incorporating multilevel SHE-PWM approach for STATCOM operation under unbalanced condition," in *Proceedings of IEEE 5th International Symposium on Power Electronics for Distributed Generation Systems*, 2014, pp. 1-7.
6. K. H. Law, W. P. Q. Ng, and K. I. Wong, "Active harmonic filtering using multilevel H-bridge inverter based STATCOM," *IOP Conference Series: Materials Science and Engineering*, Vol. 495, 2019, pp. 012036.
7. K. H. Law, W. P. Q. Ng, and P. I. Au, "Design, modelling and control implementation of PV-MPPT based DC-DC converter for STATCOM," *IOP Conference Series: Materials Science and Engineering*, Vol. 495, 2019, pp. 012035.
8. Y. Liu, H. Abu-Rub, and B. Ge, "Z-source/quasi-z-source inverters: Derived networks, modulations, controls, and emerging applications to photovoltaic conversion," *IEEE Industrial Electronics Magazine*, Vol. 8, 2014, pp. 32-44.

9. H. F. Ahmed, H. Cha, S. H. Kim, and H. G. Kim, "Switched-coupled inductor quasi-z-source inverter," *IEEE Transactions on Power Electronics*, Vol. 31, 2016, pp. 1241-1254.

10. K. H. Law, W. N. Loh, and K. I. Wong, "Mathematics derivation and simulation modelling of maximum power point tracking based controller for quasi Z source inverter," in *Proceedings of the 7th International Conference on Smart Computing and Communications*, 2019, pp. 1-5.

11. Y. W. Sia and K. H. Law, "Deep analysis of quasi Z source inverter for batteries charging and discharging capabilities across all DC capacitors' terminals," in *Proceedings of the 7th International Conference on Smart Computing and Communications*, 2019, pp. 1-5.

12. D. Sun, B. Ge, F. Z. Peng, H. A. Rub, and A. T. de Almeida, "Power flow control for quasi-z source inverter with battery based pv power generation 77 system," in *Proceedings of IEEE Energy Conversion Congress and Exposition*, 2011, pp. 1051-1056.

13. Y. Liu, B. Ge, H. Abu-Rub, A. Iqbal, and F. Peng, "Modeling and controller design of quasi-z-source inverter with battery based photovoltaic power system," in *Proceedings of IEEE Energy Conversion Congress and Exposition*, 2012, pp. 3119-3124.

14. Y. Liu, B. Ge, H. Abu-Rub, and F. Z. Peng, "Control system design of battery-assisted quasi-z-source inverter for grid-tie photovoltaic power generation," *IEEE Transactions on Sustainable Energy*, Vol. 4, 2013, pp. 994-1001.

15. D. Sun, B. Ge, W. Liang, H. Abu-Rub, and F. Z. Peng, "An energy stored quasi-z-source cascade multilevel inverter-based photovoltaic power generation system," *IEEE Transactions on Industrial Electronics*, Vol. 62, 2015, pp. 5458-5467.

16. J. Khajesalehi, K. Sheshyekani, M. Hamzeh, and E. Afjei, "High-performance hybrid photovoltaic -battery system based on quasi-z-source inverter: Application in microgrids," *IET Generation, Transmission Distribution*, Vol. 9, 2015, pp. 895-902.

17. B. Ge, Y. Liu, H. Abu-Rub, and F. Z. Peng, "State-of-charge balancing control for a battery-energy-stored quasi-z-source cascaded-multilevel-inverter-based photovoltaic power system," *IEEE Transactions on Industrial Electronics*, Vol. 65, 2018, pp. 2268-2279.

18. K. H. Law, "Mathematics modelling and simulation of batteries charging capability in quasi Z source impedance network," in *Proceedings of the 7th International Conference on Smart Computing and Communications*, 2019, pp. 1-5.

19. K. H. Law, "An effective voltage controller for quasi-Z-source inverter-based STATCOM with constant DC-link voltage," *IEEE Transactions on Power Electronics*, Vol. 33, 2018, pp. 8137-8150.

20. J. S. X. Ong, K. Y. K. Yong, K. H. Law, W. P. Q. Ng, and M. Dahidah, "CCM and DCM analysis of quasi-z-source inverter," in *Proceedings of IEEE Conference on Energy Conversion*, 2017, pp. 157-162.

21. K. H. Law. S. K. Yong, W. P. Q. Ng, and M. Dahidah, "Lead compensator design for single-phase quasi z-source inverter," *Journal of Telecommunication, Electronic and Computer Engineering*, Vol. 10, 2018, pp. 39-44.

22. K. H. Law, W. P. Q. Ng, and W. K. Wong, "Flyback cascaded multilevel inverter based SHE-PWM control for STATCOM applications," *International Journal of Power Electronics and Drive Systems*, Vol. 8, 2017, pp. 100-108.

23. K. H. Law, M. S. A. Dahidah, S. Y. Sim, W. P. Q. Ng, A. Masaoud, and A. A. Siada,

"An effective dual closed-loop scheme based on lead compensator and proportional controller for quasi z-source inverter," in *Proceedings of IEEE International Technical Conference of IEEE Region 10*, 2019, pp. 20-25.

24. K. H. Law and W. P. Q. Ng, "Dual closed-loop scheme with lead compensator and proportional controller for quasi z-source inverter based STATCOM," in *Proceedings of IEEE 7th International Conference on Power Energy*, 2019, pp. 56-61.

25. S. T. Meraj, A. Ahmed, K. H. Law, A. Arif, and A. Masaoud, "DSP based implementation of SHE-PWM for cross-switched multilevel inverter," in *Proceedings of IEEE 15th International Colloquium Signal Processing and Its Applications*, 2019, pp. 54-59.

26. S. T. Meraj, K. H. Law, and A. Masaoud, "Simplified sinusoidal pulse width modulation of cross-switched multilevel inverter," in *Proceedings of IEEE 15th International Colloquium Signal Processing and Its Applications*, 2019, pp. 1-6.

27. M. Khamar and J. Askari, "A charging method for Lithium-ion battery using min-max optimal control," in *Proceedings of the 2nd Iranian Conference on Electrical Engineering*, 2017, pp. 1239-1243.

Kah Haw Law (刘嘉豪) received his M.Eng. degree in Electrical and Electronic Engineering from the University of Nottingham, U.K. in 2010, followed by his Ph.D. degree in EEE from the University of Nottingham, Malaysia in 2015. Currently, he is a Senior Lecturer with the Department of Electrical and Computer Engineering, Curtin University, Malaysia. His research interests include renewable energy controller systems, power electronics drives, and power conversion systems. Dr. Law has received multiple IEEE Best Paper Awards in 2011, 2018, and 2019.